Sensors & Actuators: B. Chemical 427 (2025) 137150

Contents lists available at ScienceDirect

Sensors and Actuators: B. Chemical

journal homepage: www.elsevier.com/locate/snb

Cholesterol esterase-responsive near-infrared fluorescent probe for precise imaging of atherosclerosis

Jingkang Li [a], Mo Ma [a,b], Siqi Zhang [a], Wenping Dong [a], Pinyi Ma [a,*], Ziwei Zhang [a,*], Daqian Song [a]

[a] College of Chemistry, Jilin Province Research Center for Engineering and Technology of Spectral Analytical Instruments, Jilin University, Qianjin Street 2699, Changchun 130012, China
[b] School of Pharmacy, Jilin University, Qianjin Street 2699, Changchun 130012, China

ARTICLE INFO

Keywords:
Fluorescent Probe
Cholesterol esterase
Cholic acid
Lipid drop targeting
Atherosclerosis

ABSTRACT

Atherosclerosis (AS) is a common disease associated with cholesterol metabolism. Cholesterol esterase (CHE), which is found primarily in the liver, intestines, adipose tissue, and skin, plays a crucial role in cholesterol metabolism; thus, it is a potential biomarker for the early diagnosis and therapeutic monitoring of AS. Traditional fluorescent probes for detecting AS often rely on general biomarkers such as reactive oxygen species (ROS) or proteases, which lack specificity. To address this limitation, we developed a novel CHE-responsive fluorescent probe, NR-CHE, which utilizes cholic acid as the recognition group. This probe was synthesized by an esterification reaction between cholic acid and a lipid droplet-targeting near-infrared dye, NR-OH. The NR-CHE probe integrated the lipid droplet-targeting capability of NR with the specific response of CHE, thus offering a unique affinity for cells with lipid abnormalities and enabling precise imaging of atherosclerosis. *In vitro* experiments demonstrated that NR-CHE exhibited superior optical properties, with a detection limit of 0.076 U/mL. Tests involving 32 common biological interferents confirmed that the recognition group cholic acid provided high selectivity to the probe. Cell experiments further validated that NR-CHE is an effective tool for monitoring endogenous CHE in live cells. Comprehensive fluorescence imaging assessments in an AS mouse model showed that NR-CHE delivered exceptional imaging accuracy. As an extended application, NR-CHE also demonstrated potential in image-guided surgical resection in a liver cancer model. Collectively, NR-CHE holds great promise as a tool for the accurate diagnosis of AS and for guiding tumor resection surgery.

1. Introduction

Cardiovascular diseases (CVDs), which particularly affect the heart and brain, pose a major health threat due to their high mortality and disability rates[1]. Atherosclerosis (AS) is the leading cause of various types of CVDs, such as myocardial infarction, ischemic stroke, and peripheral vascular disease[2]. During AS development, oxidized low-density lipoprotein accumulates in arterial walls, forming plaques, and reactive oxygen species (ROS) and proteases can drive the disease progression[3,4]. The ability to accurately visualize the location of atherosclerotic plaques is crucial for improving the diagnosis and treatment of AS-related CVDs[5,6]. However, current diagnostic techniques often lack the specificity needed to distinguish atherosclerotic plaques from other inflammatory tissues or tumors, which also contain elevated levels of ROS and protease activity[7–10]. Therefore, there is a need to develop more specific and sensitive imaging probes that can accurately identify atherosclerotic plaques to enhance the effectiveness of surgical interventions and therapeutic monitoring.

Despite the development of various responsive fluorescent probes for detecting AS, such as those designed by Tang for detecting γ-glutamyltranspeptidase and those by Zhang for detecting cathepsin B, the widespread expression of these targeted biomarkers across different diseases limits the specificity of the probes[11–13]. This lack of specificity reduces their accuracy in distinguishing between atherosclerotic plaques and other tissue abnormalities. In contrast, cholesterol esterase (CHE), also known as cholesterol hydrolase, offers greater specificity in the context of AS. CHE plays a crucial role in cholesterol metabolism by hydrolyzing cholesterol esters, which are directly involved in plaque formation[14,15]. This enzyme is more closely associated with the pathological processes of AS; for this reason, it is a promising biomarker

* Corresponding authors.
E-mail addresses: mapinyi@jlu.edu.cn (P. Ma), zzw@jlu.edu.cn (Z. Zhang).

https://doi.org/10.1016/j.snb.2024.137150
Received 1 October 2024; Received in revised form 28 November 2024; Accepted 16 December 2024
Available online 17 December 2024
0925-4005/© 2024 Elsevier B.V. All rights are reserved, including those for text and data mining, AI training, and similar technologies.

for more accurate imaging. However, to date, CHE-targeting fluorescent probes for AS imaging have not been developed.

To address the issue of insufficient specificity in existing fluorescent probes, a novel probe with high specificity and sensitivity for the detection of CHE in AS was designed and synthesized. We selected Nile Red, a commercially available lipid droplet dye, as the fluorophore due to its intrinsic imaging capability for AS plaques[16,17]. By covalently linking Nile Red with the recognition group cholic acid, we developed a fluorescent probe, NR-CHE, that had high specificity for AS (Scheme 1). We systematically studied the probe's responsiveness to AS and subsequently applied it in imaging studies in AS models to explore its potential for precise plaque visualization and improved surgical navigation.

2. Experimental methods

2.1. Synthesis of probe

Detailed information regarding reagents, instruments, and other materials utilized in the synthesis is provided in the Supplementary Material. The synthesis pathway is depicted in Fig. 1. The key intermediates and final synthetic products were thoroughly characterized using ^{1}H, ^{13}C-NMR and MS, as shown in Figure S1-S6.

Synthesis of NR-OH. Compound 1 was synthesized according to the method reported in the literature[18]. Compound 1 (165 mg, 1 mmol) and 2,6-dihydroxynaphthalene (240 mg, 1.5 mmol) were dissolved in 2 mL of DMF, and the mixture was stirred overnight at 150 °C. After cooling to room temperature, 40 mL of saturated salt water and ethyl acetate were added to the solution to extract the organic layer. The mixture was purified by silica gel chromatography (petroleum ether: ethyl acetate = 3:1). The resulting compound, NR-OH, was obtained as a dark red solid with a 20 % yield. ^{1}H NMR (600 MHz, DMSO-d_6) δ 10.40 (s, 1 H), 7.97 (d, J = 8.6 Hz, 1 H), 7.88 (d, J = 2.5 Hz, 1 H), 7.56 (d, J = 9.0 Hz, 1 H), 7.09 (d, J = 11.1 Hz, 1 H), 6.78 (d, J = 11.8 Hz, 1 H), 6.62 (d, J = 2.7 Hz, 1 H), 6.14 (s, 1 H), 3.49 (q, J = 7.0 Hz, 4 H), 1.16 (t, J = 7.1 Hz, 6 H). ^{13}C NMR (151 MHz, DMSO-d_6) δ 182.02, 161.06, 152.05, 151.13, 146.86, 139.19, 134.21, 131.26, 127.91, 124.32, 118.81, 110.35, 108.58, 104.55, 96.50, 44.88, 12.92. MS data (LC-ESI-MS, m/z) for $C_{16}H_{10}NO_3^+$ $[M+H]^+$: calculated, 335.1390; found: 335.1399. (Figure S1 – S3)

Synthesis of NR-CHE. Cholic acid (408 mg, 1 mmol) was dissolved in 15 mL of anhydrous DMF, and while stirring, triethylamine (100 μL, 0.7 mmol) was added. After HBTU (378 mg, 1 mmol) was gradually added, the mixture was stirred for 3 h. Subsequently, NR-OH (117 mg, 0.4 mmol) was added, and the reaction mixture was further stirred at room temperature overnight. Upon completion, the mixture was diluted with saturated NaCl solution and then extracted with ethyl acetate. The organic layer was separated, dried over anhydrous sodium sulfate, and then concentrated under reduced pressure. Purification was carried out by silica gel column chromatography (dichloromethane:methanol = 20:1), which yielded NR-CHE as a purple-black solid with a 21 % yield. ^{1}H NMR (600 MHz, DMSO-d_6) δ 8.20 (d, J = 2.3 Hz, 1 H), 8.16 (d, J = 8.5 Hz, 1 H), 7.60 (d, J = 9.1 Hz, 1 H), 7.44 (dd, J = 8.5, 2.3 Hz, 1 H), 6.82 (dd, J = 9.2, 2.5 Hz, 1 H), 6.66 (d, J = 2.6 Hz, 1 H), 6.27 (s, 1 H), 4.32 – 4.30 (m, 2 H), 4.16 (d, J = 3.4 Hz, 1 H), 4.10 (d, J = 3.4 Hz, 1 H), 4.02 – 3.99 (m, 2 H), 3.77 (d, J = 2.6 Hz, 1 H), 3.50 (d, J = 7.2 Hz, 4 H), 2.20 (dd, J = 15.2, 9.4 Hz, 3 H), 2.03 – 1.96 (m, 2 H), 1.88 – 1.78 (m, 6 H), 1.65 (dd, J = 16.3, 8.0 Hz, 5 H), 1.43 (d, J = 13.1 Hz, 6 H), 1.16 (d, J = 7.1 Hz, 6 H), 1.03 (d, J = 6.0 Hz, 4 H), 0.81 (d, J = 10.1 Hz, 5 H). ^{13}C NMR (DEPTQ) (151 MHz, DMSO-d_6) δ 181.59, 172.59, 153.46, 152.56, 151.54, 147.08, 137.98, 133.58, 131.46, 129.20, 127.52, 124.72, 124.28, 116.39, 110.85, 104.80, 96.50, 71.46, 70.91, 66.72, 51.65, 46.54, 46.23, 44.99, 42.00, 41.85, 35.79, 35.50, 35.35, 34.86, 31.27, 31.02, 30.89, 29.01, 27.80, 27.74, 26.69, 23.28, 23.08, 17.50, 17.38, 12.92.MS data (LC-ESI-MS, m/z) for $C_{44}H_{56}N_2O_7^+$ $[M+H]^+$: calculated, 725.4160; found: 725.4156. (Figure S4 – S6)

2.2. Detection of CHE in solution

A 1 mM NR-CHE stock solution was prepared by dissolving the synthesized NR-CHE in DMSO. To optimize the enzymatic reaction conditions, various parameters were systematically adjusted. The photophysical properties of the NR-CHE probe were thoroughly examined under different reaction times, temperatures, and pHs.

2.3. Imaging in cells

To investigate the behavior of CHE at the cellular level, LO2, HepG2, and RAW 264.7 cell lines were used. These cells were cultured on glass-bottom dishes for 24 h to allow for real-time imaging of CHE activity. Specifically, to mimic the cellular environment associated with atherosclerosis (AS), RAW 264.7 cells were induced into foam cells using oxidized low-density lipoprotein (ox-LDL)[19]. The successful induction of foam cells was verified by measuring the expression level of CD40 using an appropriate assay kit[12]. For cell imaging experiments, a Nikon AX laser scanning confocal microscope was employed, and the imaging was conducted using an excitation wavelength of 580 nm.

CHE Dynamics in RAW 264.7 Cells and Foam Cells. To model foam

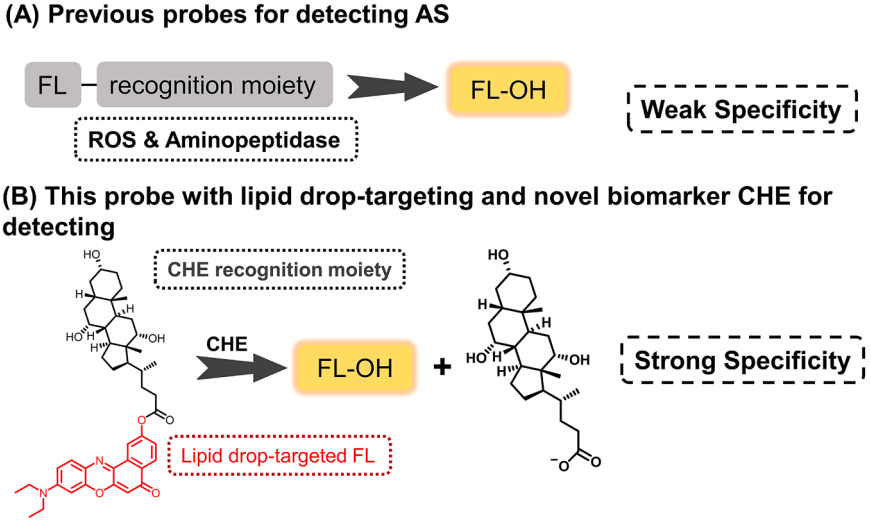

Scheme 1. Mechanism in enzyme digestion response of probes.

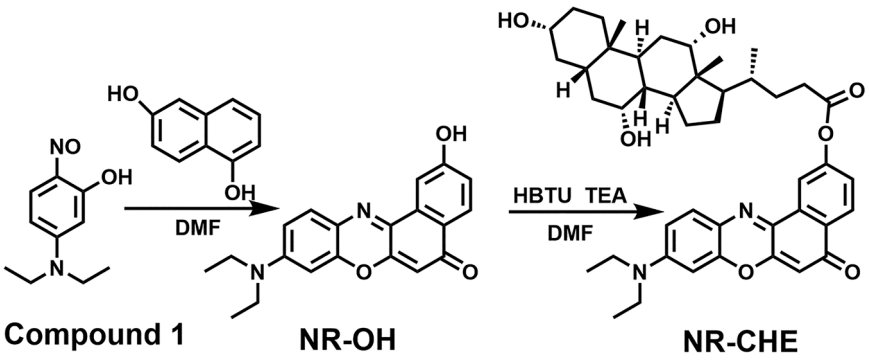

Fig. 1. Synthetic route of NR-CHE probe.

cells, RAW 264.7 cells were treated with 20 μg/mL of oxidized low-density lipoprotein (ox-LDL) and cultured for 24 h[13]. Morphological changes, which are indicative of foam cell formation, were observed under a microscope. Subsequently, time-lapse imaging of RAW 264.7 cells and foam cells treated with 10 μM NR-CHE was performed to monitor CHE dynamics at various time points. This enabled the detailed study of CHE activity during the transformation of macrophages into foam cells, which is a critical process in atherosclerosis development [20].

CHE Dynamics in HepG2 and LO2 Cells. Initial experiments involved time-lapse imaging of HepG2 and LO2 cells treated with 10 μM NR-CHE to monitor CHE dynamics. Using Donepezil as an enzyme inhibitor, cell imaging experiments were performed. Cells were first pre-treated with 1 mM Donepezil for 8 h, washed three times with PBS (10 mM, pH 7.4), and then incubated with 10 μM NR-CHE before imaging. This approach allowed for the real-time observation of CHE activity within these cell lines to provide insights into the differential behavior of CHE in cancerous versus normal liver cells.

2.4. Establishment of mouse model

All animal experiments were conducted in accordance with the ethical guidelines set by the Institutional Animal Care and Use Committee (IACUC) of Jilin University, under the ethical permit number SY20230631. The disease models were established using ApoE^{-}/$^{-}$/HF and BALB/c-nu mice.

AS mouse model. A mouse model of AS was developed based on the methodologies documented in the literature[12,21]. The induction involved a 12-week regimen of a methionine and choline-deficient diet to simulate high-fat dietary conditions. Histological analyses, including Hematoxylin and Eosin (H&E) staining, were used to confirm establishment of the AS model.

In Situ Imaging and Fluorescence-Mediated Surgical Resection. To induce tumor growth, a suspension of HepG2 cells (approximately 1×10^7 cells in 50 μL of PBS) was subcutaneously injected into the right flank of each BALB/c-nu mouse, and tumors were allowed to develop over the course of approximately two weeks[22]. For *in situ* imaging, mice bearing HepG2 tumors were administered NR-CHE (50 μM, 200 μL) via intratumoral injection[23]. Fluorescence imaging was conducted at 5-min intervals following the injection. A control group was also injected with NR-CHE injections, and imaging was performed using a small animal imager to monitor the fluorescence signals. To facilitate fluorescence-mediated surgical resection, the tumor-bearing mouse was dissected after the intratumoral injection before being subjected to fluorescence imaging. Guided by the fluorescent images, the tumor was surgically excised, and the mouse was re-imaged to confirm the resection. Additionally, main organs including the heart, liver, spleen, lungs, and kidneys, as well as the HepG2 tumor, were collected post-surgery for further fluorescence imaging to assess the distribution and specificity of the NR-CHE probe.

3. Results and discussion

3.1. Design principle of NR-CHE

The development of AS involves a persistent inflammatory response that ultimately leads to lipid accumulation and plaque formation[24]. Cholesterol is essential for maintaining vital body functions, but elevated cholesterol levels can contribute to the development of AS[25]. Therefore, we aimed to assess the progression of AS through the fluorescence detection of CHE *in vivo*. To construct a strong AS-specific probe, NR was first selected a fluorescent dye due to its lipid droplet targeting ability. We tried to introduce hydroxyl groups in the NR aromatic ring at position 2, which further strengthened the original ICT effect of the molecule and significantly enhanced the fluorescence intensity of the molecule (Figure S7). However, since the active group of cholesterol molecule is hydroxyl, it cannot form ester bonds with NR-OH that cannot be severed by esterase. Cholic acid lies in one of the metabolic pathways of cholesterol, and the two molecules are very similar in structure[26]. Additionally, the exposed carboxyl group of cholic acid is highly suitable for constructing our probe. In summary, the organic fluorescence probe was constructed using cholic acid as the recognition group and NR-OH as the fluorophore. The two molecules were linked by ester bonds to allow for the specific detection of CHE in AS imaging.

To validate the reaction mechanism of NR-CHE in detecting CHE, the reaction solution was characterized by HPLC and MS. Initially, HPLC was employed to observe changes in the presence and absence of CHE. As shown in Fig. 2B, the retention times for NR-CHE and NR-OH were 1.2 min and 4.7 min, respectively. Upon interacting with CHE, a significant decrease in the peak at 4.7 min was observed, accompanied by the appearance of a new peak at 1.2 min. The characteristics of the peak at 1.2 min were identical to those of NR-OH, an indication that NR-CHE was hydrolyzed by CHE to produce NR-OH. Furthermore, the enzymatic reaction was analyzed by mass spectrometry, as illustrated in Fig. 2 C. Both NR-CHE and NR-OH were detected in the mass spectrum, which corroborates the HPLC results. These findings are consistent across HPLC and MS and confirm that NR-CHE was hydrolyzed by CHE, resulting in the formation of NR-OH. In addition to these experimental validations, molecular docking studies further provided evidence that the probe could effectively recognize the recognition site on CHE. As depicted in Fig. 2D, the molecular docking simulation demonstrated that NR-CHE forms three hydrogen bonds with ARG-63 and TYR-103 of CHE. The calculated binding energy of −9.9 kcal/mol suggests a strong affinity between NR-CHE and CHE, which underscores the probe's capability to effectively engage with its target enzyme[27].

3.2. Optical properties of NR-CHE

To further investigate the photophysical properties of the NR-CHE probe, we first optimized experimental conditions, including time, temperature, and pH. Following the optimization, the absorption and

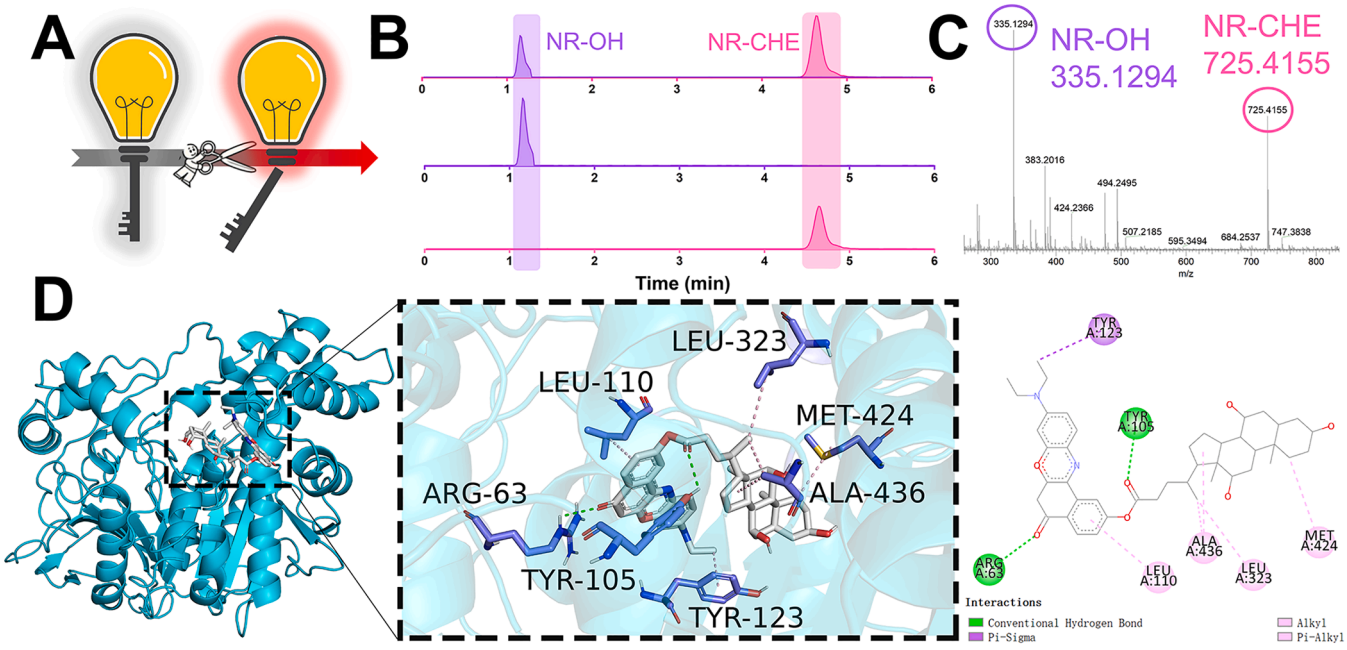

Fig. 2. Characterization of enzymatic reaction mechanism and theoretical calculation. (A) Schematic diagram of enzyme digestion response. (B) Characterization by HPLC-MS. (C) Characterization of enzymatic reaction solution by mass spectrometry. (D) Molecular docking simulation of the binding between NR-CHE and CHE.

fluorescence spectra of NR-CHE, both before and after the reaction with CHE, were analyzed under optimal conditions (Fig. 3 A).

Time Optimization. The reaction time was first optimized. As depicted in Figure S8, in the presence of CHE (0.6 U/mL), the fluorescence intensity of the NR-CHE solution (λ_{emmax} = 690 nm) increased progressively as the reaction time was extended, until eventually reaching an equilibrium. To ensure the completion of the enzymatic reaction, 120 min was selected as the optimal reaction time.

pH Optimization. The pH of the NR-CHE solution was optimized. As shown in Figure S9, under acidic conditions, the NR-CHE solution exhibited high fluorescence intensity at λ_{emmax} = 690 nm. This high intensity persisted even as the solution pH approached the neutral pH. However, when the solution was alkaline, the fluorescence intensity decreased significantly. These results indicate that CHE activity is not

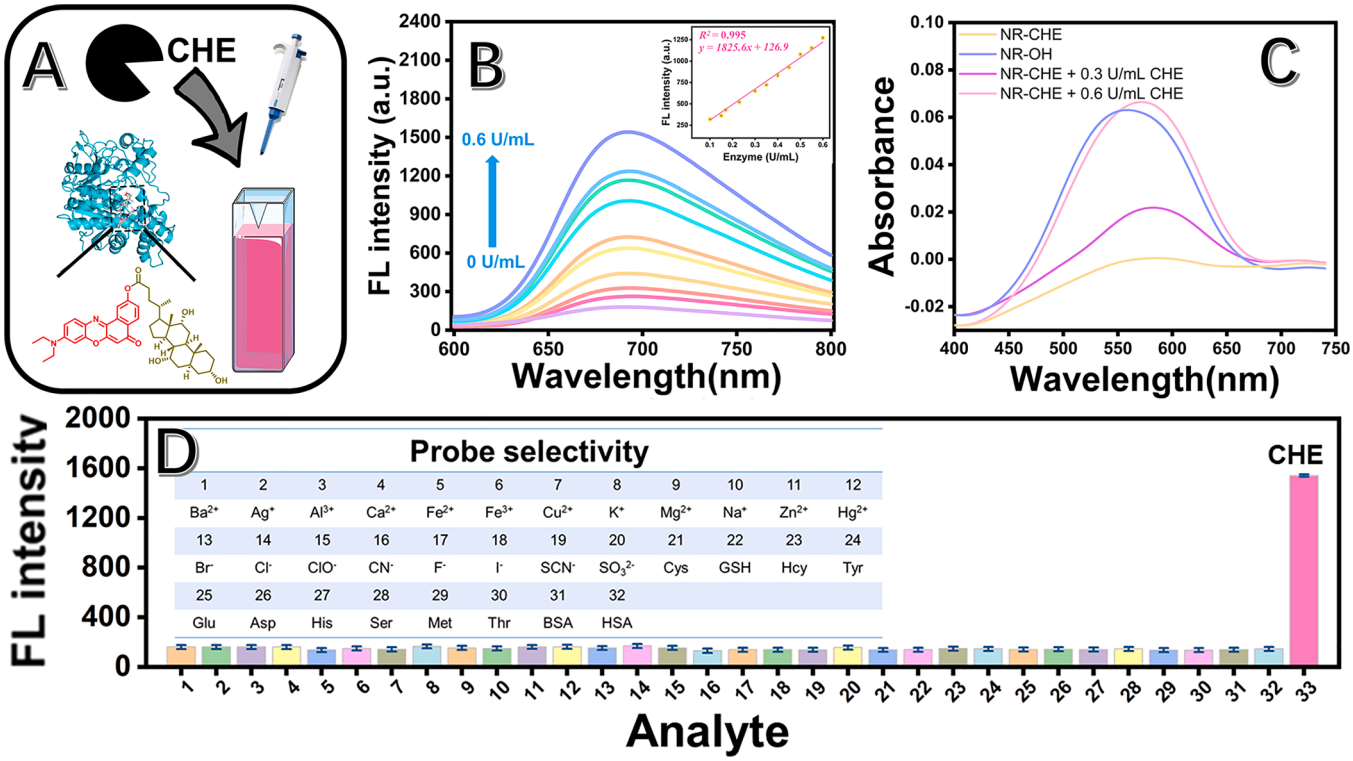

Fig. 3. (A) Diagram of *in vitro* reaction. (B) Fluorescence spectra (λ_{emmax} = 690 nm) of reaction between 10 μM NR-CHE and 0–0.6 U/mL CHE. (C) Ultraviolet absorption spectrum of NR-CHE, NR-OH and reaction solution. (D) Fluorescence intensity of 10 μM NR-CHE in the presence of various analytes (1 mM, unless otherwise stated).

significantly affected by a non-alkaline environment. Therefore, to best simulate the physiological conditions and guide subsequent cell experiments, a pH of 7.4 was chosen as the optimal pH.

Temperature Optimization. The solution temperature was optimized. As shown in Figure S10, in the absence of an enzyme, the fluorescence intensity of both the NR-OH fluorophore and the NR-CHE probe remained relatively stable across different temperatures. A slight decrease in the fluorescence intensity was, however, observed at high temperatures. In the presence of the enzyme, the fluorescence intensity fluctuated within a certain range as the temperature was varied, which is similar to the trend of the fluorophore alone. This suggests that higher temperatures lead to reduced fluorescence intensity and decreased enzyme activity. Based on these findings, 37°C was selected as the optimal temperature for subsequent experiments.

Spectral Response to CHE. First, the UV absorption spectra of the probe and its reaction with CHE were measured. As can be observed in the absorption spectrum (Fig. 3 C), the absorption peak at 580 nm of the probe in the presence of CHE was significantly enhanced, and the peak type and intensity were also consistent with those of the fluorophore NR-OH. This observation demonstrates that the NR-CHE probe could be recognized by CHE and hydrolyzed to produce the fluorophore. Then, at an excitation wavelength of 580 nm, the fluorescence intensity at 690 nm of the probe in the presence of CHE was significantly enhanced (Fig. 3B). This further verifies that using a spectroscopic method, the probe NR-CHE could detect CHE. Then, the sensitivity and the selectivity were evaluated. The fluorescence intensity exhibited a strong linear relationship with CHE concentration in the range of 0–0.6 U/mL ($y = 1825.6x + 126.9$, $R^2 = 0.995$) (Figure S11). The detection limit concerning CHE was determined to be 0.076 U/mL. These results demonstrate that NR-CHE is highly sensitive to CHE and therefore is suitable for the quantitative detection of CHE activity.

Selectivity of NR-CHE to CHE. To evaluate whether NR-CHE can selectively image CHE in complex biological systems, we examined the fluorescence spectra of NR-CHE after being co-incubated with various bioactive molecules. As illustrated in Fig. 3D, following the incubation with NR-CHE, a significant increase in fluorescence intensity was observed only when CHE was present; other analytes caused no substantial change. This indicates that NR-CHE has excellent selectivity for CHE, confirming its potential for selective fluorescent imaging of CHE in biological systems.

3.3. Fluorescence imaging of CHE in cells

Encouraged by its *in vitro* fluorescence imaging capabilities, the NR-CHE probe was further employed to detect intracellular CHE activity. Prior to the imaging, the cytotoxicity of NR-CHE to RAW 264.7 macrophage cells were evaluated using a standard MTT assay (Figure S12). Additionally, a hemolysis test was employed to confirm that NR-CHE had a low hemolysis rate and high biocompatibility (Figure S13).

Previous studies have demonstrated that during the development of AS, CD40 is commonly expressed in arterial plaques within various cell

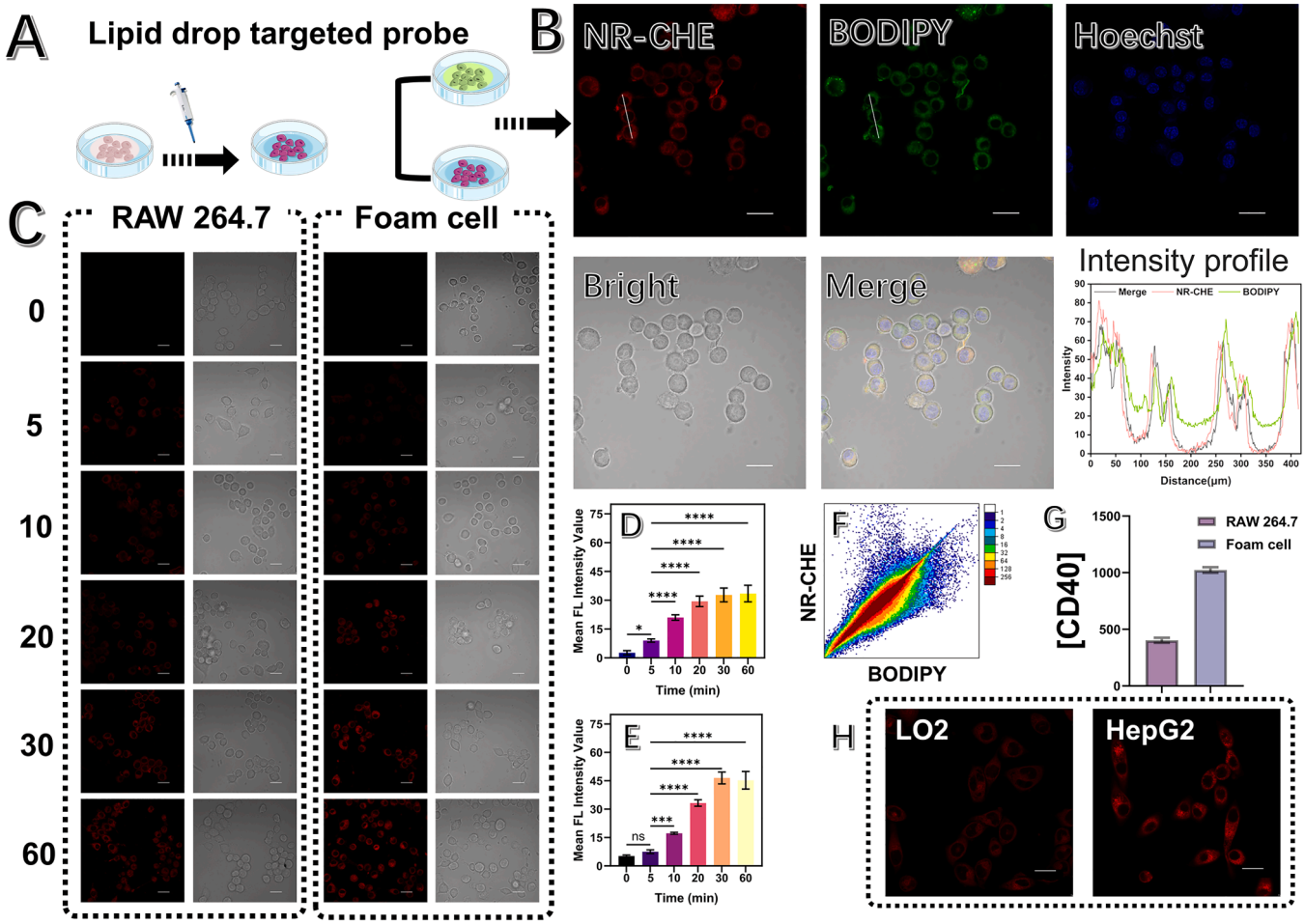

Fig. 4. (A) Diagram showing cell imaging procedures. (B) Cellular colocalization imaging of NR-CHE ($\lambda_{ex} = 580$ nm, $\lambda_{emmax} = 690$ nm) and commercial lipid droplet-targeting dye BODIPY($\lambda_{ex} = 493$ nm, $\lambda_{emmax} = 503$ nm). (C) Time-dependent fluorescence imaging (0, 5, 10, 20, 30, 60 min). (D) Mean fluorescence intensity of RAW 264.7 cells. (E) Mean fluorescence intensity of foam cells. (F) Colocalization scatter plot. (G) Content of CD40 in RAW 264.7 and foam cells. (H) Images of LO2 and HepG2 cells. Scale bar = 20 μm.

types, including foam cells, smooth muscle cells, and T cells[28]. To replicate this environment, the transformation of RAW 264.7 cells into foam cells was induced using oxidized low-density lipoprotein (ox-LDL) [12]. The successful transformation was verified by measuring CD40 expression levels using a commercial CD40 detection kit. As shown in Fig. 4 G, the CD40 content in the foam cells significantly increased, which confirms that the macrophages were successfully transformed into foam cells.

Subsequently, we utilized NR-CHE to image endogenous CHE in cells. The probe NR-CHE (10 μM) was added to the foam cells, and fluorescence imaging was conducted using a confocal microscope. The fluorescence intensity of NR-CHE increased significantly with increasing incubation time and was stabilized after 30 minutes (Fig. 4 C). This establishes 30 minutes as the optimal incubation time for NR-CHE in cells. The fluorescence intensity was significantly higher in foam cells compared to that in RAW 264.7 cells, which is indicative of elevated CHE levels in foam cells. To further confirm the lipid droplet-targeting capability of NR-CHE, colocalization imaging was performed using the commercial lipid droplet-targeting dye BODIPY[29]. Fig. 4B shows that the regions of interest for NR-CHE and BODIPY coincided, and this region was completely different from the region of the blue nuclear dye [30]. According to the calculations, the Pearson's coefficient was as high as 0.977. As can be seen in Fig. 4 F, the co-localization scatter plot showed that the two dyes were very close to the diagonal[31]. This result proves that the degree of co-location of the two dyes is very high, affirming the probe can effectively target the lipid droplets.

Finally, to explore the broader application of NR-CHE, normal liver cells (LO2) and hepatoma cells (HepG2) were incubated with NR-CHE for 30 minutes before fluorescence imaging. As shown in Fig. 4H, the fluorescence intensity of HepG2 cells significantly increased, demonstrating that NR-CHE can be used for the imaging of hepatoma cells. In order to further verify the specificity of NR-CHE to CHE , donepezil was selected as an inhibitor of CHE. The experimental results proved that the fluorescence intensity was no longer obvious in the experimental group adding the inhibitor, while the blank control group was consistent with the original experimental results (Figure S14).

3.4. Application of NR-CHE in AS diagnosis

Apolipoprotein E-knockout mice on a high-fat diet (ApoE^{-}/$^{-}$/HF), with feeding durations of 0, 4, 8, and 12 weeks, were used as a model for AS. The expression level of CD40, a conventional biomarker of early AS, was measured using a mouse CD40 ELISA kit and used to monitor the progression of atherosclerotic plaques[28]. As shown in Fig. 5 C, the CD40 levels gradually increased with increasing feeding time, which confirms the successful establishment of an early-AS mouse model. This was further validated by hematoxylin and eosin (H&E) staining, as shown in Fig. 5b_1 and Fig. 5b_2. The H&E-stained sections revealed a substantial presence of foam cells with vacuolated cytoplasm on the surface, along with necrotic material, deposited lipids, and cholesterol crystals in deeper layers; all of which are indicative of the successful establishment of an AS model[32].

Following the model validation, the fluorescence intensity of NR-CHE in the aorta of ApoE^{-}/$^{-}$/HF mice fed at different feeding

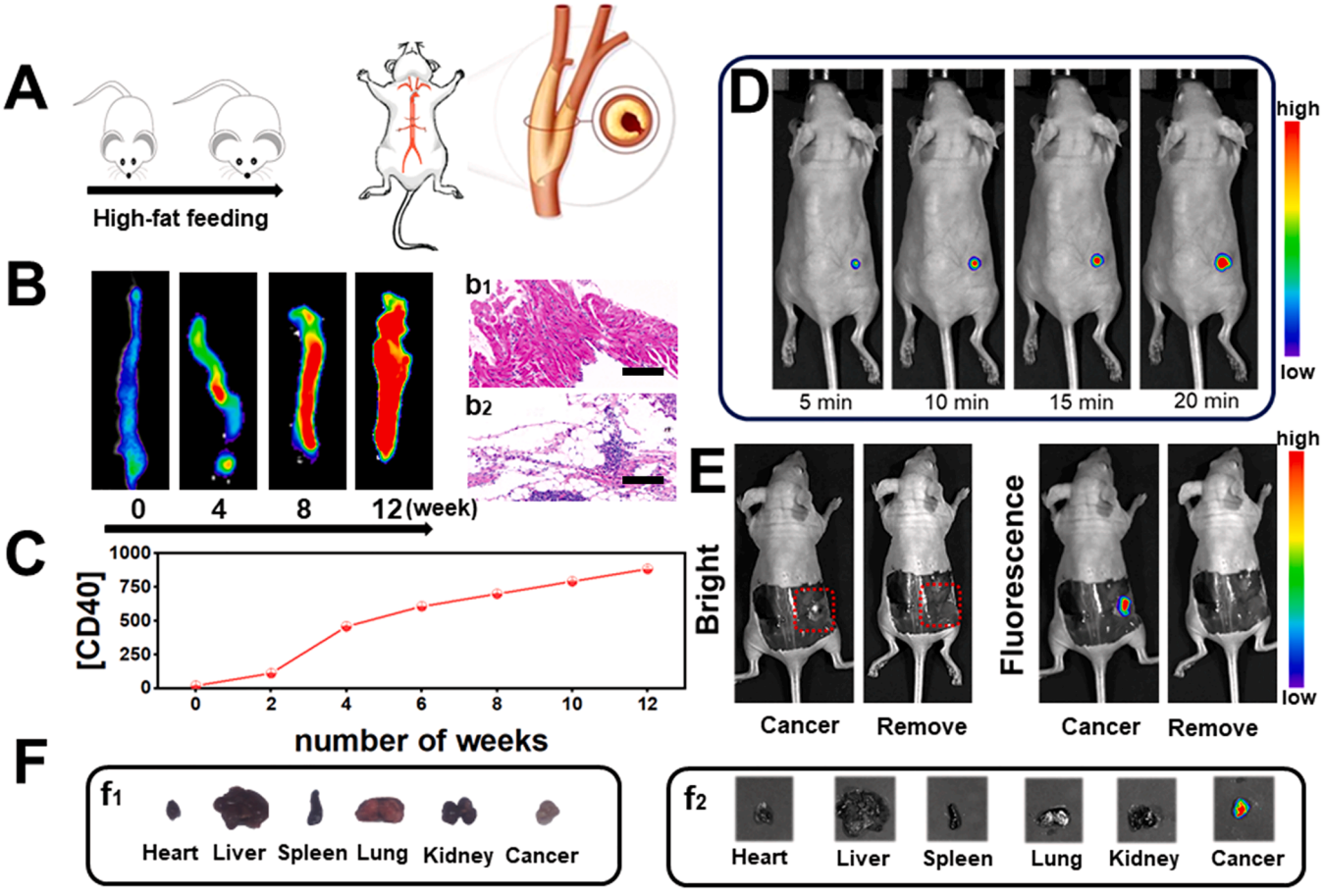

Fig. 5. (A) Diagram representing the establishment of the disease mouse model. (B) Imaging and H&E staining of mouse aorta: (b_1) the pathological staining of the aorta of normal mice, and (b_2) the pathological staining of the aorta of mice fed with a high-fat diet for 8 weeks. Scale bar = 100 μm. (C) Content of CD40 in the blood of mice. (D) Images of HepG2 tumor-bearing mouse. (E) Comparison of images before and after tumor resection. (F) Images of main internal organs and HepG2 tumor (f_1 is an actual picture, and f_2 is a fluorescence image).

intervals was monitored using an AniView SE small animal imaging system. As shown in Fig. 5B, the fluorescence intensity in the atherosclerotic regions of the aorta significantly increased with the increase of high-fat diet feeding durations. The conspicuous red fluorescence areas indicated the presence of plaques, which is demonstrative of the severity of AS. The use of NR-CHE, a lipid droplet-targeting molecular probe, enables more accurate imaging of AS and provides more precise predictions of plaque formation. With an ability to specifically detect the increase of CHE activity in the blood vessels of ApoE^{-}/$^{-}$/HF mice. The distinct red fluorescence at plaque sites allows for the monitoring of the formation of atherosclerotic plaques.

3.5. Application of NR-CHE in liver cancer diagnosis

To explore the broader applications of NR-CHE, we utilized it in imaging of liver cancer and further evaluated its potential for image-guided surgical resection (Fig. 5E). Initially, fluorescence imaging on a tumor-bearing mouse was performed. After 20 minutes, a distinct fluorescent signal was observed at the tumor site (Fig. 5D). Guided by the fluorescence, the tumor was surgically removed (Fig. 5E). Following the excision of the fluorescent tissue, no residual fluorescence was detected in the mouse, an indication that the tumor was successfully resected. Furthermore, as shown in Fig. 5 F, the tumor exhibited strong red fluorescence, whereas the heart, liver, spleen, lungs, and kidneys did not. This contrasting observation suggests that the CHE activity is significantly higher at the tumor site, thereby allowing NR-CHE to effectively distinguish cancerous tumors from normal tissues. In summary, the NR-CHE probe demonstrates significant potential as a powerful contrast chemosensor for assisting in the surgical resection of liver cancer in clinical settings. This probe can be utilized as a tool for enhancing surgical precision and outcomes.

4. Conclusion

This study introduces NR-CHE, which is a novel lipid droplet-targeting fluorescent dye specifically designed to detect CHE. Our findings demonstrate that NR-CHE is a new highly sensitive and specific method for identifying AS. The fluorescence response of the probe was linearly correlated with CHE concentration, and the detection limit was as low as 0.076 U/mL, which highlights the potential of NR-CHE in quantitative analysis in both research and clinical settings. The data showed a strong correlation between fluorescence intensity and AS progression in ApoE^{-}/$^{-}$/HF mice. NR-CHE was successfully used for image-guided surgical resection in liver cancer models, which underscores its broader applicability. NR-CHE was able to distinguish between cancerous and normal tissues through different fluorescence intensities, an indication that it can be a powerful tool for enhancing the precision of oncological surgeries. Future work could involve expanding the application of NR-CHE to other lipid metabolism-related diseases and investigating its potential role in monitoring therapeutic responses. Additionally, studies could further explore the utilizability of the probe in detecting early-stage disease markers. Overall, this study offers a new avenue for the early diagnosis and intervention of CHE-related disorders.

CRediT authorship contribution statement

Daqian Song: Supervision, Resources, Project administration, Funding acquisition. **Ziwei Zhang:** Software, Resources, Methodology. **Pinyi Ma:** Writing – review & editing, Software, Project administration, Data curation. **Wenping Dong:** Investigation. **Siqi Zhang:** Investigation, Data curation. **Mo Ma:** Investigation, Data curation. **Jingkang Li:** Writing – original draft, Validation, Investigation, Data curation, Conceptualization.

Declaration of Competing Interest

The authors declare that they have no known competing financial interests or personal relationships that could have appeared to influence the work reported in this paper.

Acknowledgments

This work was supported by the National Natural Science Foundation of China (22004046 and 22074052) and the Science and Technology Developing Foundation of Jilin Province of China (20240404044ZP).

Appendix A. Supporting information

Supplementary data associated with this article can be found in the online version at doi:10.1016/j.snb.2024.137150.

Data availability

Data will be made available on request.

References

[1] X.X. Fang, H. Ardehali, J.X. Min, F.D. Wang, The molecular and metabolic landscape of iron and ferroptosis in cardiovascular disease, Nat. Rev. Cardiol. 20 (2023) 7–23.
[2] J.L.M. Björkegren, A.J. Lusis, Atherosclerosis: recent developments, Cell 185 (2022) 1630–1645.
[3] G.J. Koelwyn, E.M. Corr, E. Erbay, K.J. Moore, Regulation of macrophage immunometabolism in atherosclerosis, Nat. Immunol. 19 (2018) 526–537.
[4] C.L. Liu, J. Guo, X. Zhang, G.K. Sukhova, P. Libby, G.P. Shi, Cysteine protease cathepsins in cardiovascular disease: from basic research to clinical trials, Nat. Rev. Cardiol. 15 (2018) 351–370.
[5] E.R.H. Walter, S.M. Cooper, J.J. Boyle, N.J. Long, Enzyme-activated probes in optical imaging: a focus on atherosclerosis, Dalton Trans. 50 (2021) 14486–14497.
[6] W. Chen, M. Schilperoort, Y.H. Cao, J.J. Shi, I. Tabas, W. Tao, Macrophage-targeted nanomedicine for the diagnosis and treatment of atherosclerosis, Nat. Rev. Cardiol. 19 (2022) 228–249.
[7] K. Wang, X.Y. Chen, W.D. Liu, Y. Yue, X.L. Wen, Y.S. Yang, et al., Imaging investigation of hepatocellular carcinoma progress via monitoring γ-glutamyltranspeptidase level with a near-infrared fluorescence/photoacoustic bimodal probe, Anal. Chem. 95 (2023) 14235–14243.
[8] Y.J. Kim, S.J. Park, C.S. Lim, D.J. Lee, C.K. Noh, K. Lee, et al., Ratiometric detection of γ-glutamyltransferase in human colon cancer tissues using a two-photon probe, Anal. Chem. 91 (2019) 9246–9250.
[9] A. Corti, E. Belcastro, S. Dominici, E. Maellaro, A. Pompella, The dark side of gamma-glutamyltransferase (GGT): Pathogenic effects of an 'antioxidant' enzyme, Free Radic. Biol. Med. 160 (2020) 807–819.
[10] Y.Z. Shen, T.T. Wu, Y.Q. Wang, S.L. Zhang, X.L. Zhao, H.Y. Chen, et al., Nucleolin-targeted ratiometric fluorescent carbon dots with a remarkably large emission wavelength shift for precise imaging of cathepsin B in living cancer cells, Anal. Chem. 93 (2021) 4042–4050.
[11] Y. Ma, J.H. Shang, L.H. Liu, M.H. Li, X.Y. Xu, H. Cao, et al., Rational design of a double-locked photoacoustic probe for precise in vivo imaging of cathepsin B in atherosclerotic plaques, J. Am. Chem. Soc. 145 (2023) 17881–17891.
[12] H. Wang, X.T. Zhang, P. Li, F. Huang, T.C. Xiu, H.T. Wang, et al., Prediction of early atherosclerotic plaques using a sequence-activated fluorescence probe for the simultaneous detection of γ-glutamyl transpeptidase and hypobromous acid, Angew. Chem. Int. Ed. 63 (2024) e202315861.
[13] X.Q. Huang, S.Y. Zhang, W. Fu, L.P. Wang, Z.H. Liu, Y. Tang, et al., In situ imaging of GGT and HOBr-triggered atherosclerotic plaque rupture via activating the RunX2/Col IV signaling pathway, Anal. Chem. 96 (2024) 4138–4145.
[14] M.E. Vaquero, J. Barriuso, M.J. Martínez, A. Prieto, Properties, structure, and applications of microbial sterol esterases, Appl. Microbiol. Biotechnol. 100 (2016) 2047–2061.
[15] N. Weber, P. Weitkamp, K.D. Mukherjee, Steryl and stanyl esters of fatty acids by solvent-free esterification and transesterification in vacuo using lipases from Rhizomucor miehei, Candida antarctica, and Carica papaya, J. Agric. Food Chem. 49 (2001) 5210–5216.
[16] F. Zhang, X.X. Wu, B. Liu, T. Han, D.Y. Yan, D. Wang, et al., Emerging designs of aggregation-induced emission luminogens for lipid droplets imaging, Coord. Chem. Rev. 493 (2023) 215337.
[17] R. Zhou, C.G. Wang, X.S. Liang, F.M. Liu, P. Sun, X. Yan, et al., A new organic molecular probe as a powerful tool for fluorescence imaging and biological study of lipid droplets, Theranostics 13 (2023) 95–105.
[18] K.Y. Liu, X.Q. Kong, Y.Y. Ma, W.Y. Lin, Preparation of a Nile Red-Pd-based fluorescent CO probe and its imaging applications in vitro and in vivo, Nat. Protoc. 13 (2018) 1020–1033.

[19] T. Laval, M. Ouimet, A role for lipophagy in atherosclerosis, Nat. Rev. Cardiol. 20 (2023) 431–432.
[20] D.D. Wang, Y. Yang, Y.N. Lei, N.T. Tzvetkov, X.D. Liu, A.W.K. Yeung, et al., Targeting foam cell formation in atherosclerosis: therapeutic potential of natural products, Pharmacol. Rev. 71 (2019) 596–670.
[21] Y.H. Goo, J.P. Ayyappan, F.D. Cheeran, S. Bangru, P.K. Saha, P. Baar, et al., Lipid droplet-associated hydrolase mobilizes stores of liver X receptor sterol ligands and protects against atherosclerosis, Nat. Commun. 15 (2024) 6540.
[22] L.L. Xu, M. Ma, J.K. Li, H. Yang, D.J. Gao, P.Y. Ma, et al., Exploring butyrylcholinesterase expression in diseases using a promising fluorescent imaging tool, Sens Actuators B Chem. 394 (2023) 134432.
[23] S.Q. Zhang, M. Ma, C. Zhao, J.K. Li, L.L. Xu, Z.H. Zhang, et al., A novel low-background nitroreductase fluorescent probe for real-time fluorescence imaging and surgical guidance of thyroid cancer resection, Biosens. Bioelectron. 261 (2024) 116514.
[24] D. Wolf, K. Ley, Immunity and inflammation in atherosclerosis, Circ. Res. 124 (2019) 315–327.
[25] F.L. Gong, Z.B. Wang, R. Mo, Y.T. Wang, J. Su, X.L. Li, et al., Nano-sponge-like liposomes remove cholesterol crystals for antiatherosclerosis, J. Control. Release 349 (2022) 940–953.
[26] D. Gaillard, D. Masson, E. Garo, M. Souidi, J.P.P. de Barros, K. Schoonjans, et al., Muricholic acids promote resistance to hypercholesterolemia in cholesterol-fed mice, Int. J. Mol. Sci. 22 (2021) 7163.
[27] L.L. Xu, H.Y. Chu, D.J. Gao, Q. Wu, Y. Sun, Z.X. Wang, et al., Chemosensor with ultra-high fluorescence enhancement for assisting in diagnosis and resection of ovarian cancer, Anal. Chem. 95 (2023) 2949–2957.
[28] F. Mach, U. Schonbeck, G.K. Sukhova, E. Atkinson, P. Libby, Reduction of atherosclerosis in mice by inhibition of CD40 signalling, Nature 394 (1998) 200–203.
[29] J.X. Hong, Y.J. Liu, X.D. Tan, G.Q. Feng, Engineering of a NIR fluorescent probe for high-fidelity tracking of lipid droplets in living cells and nonalcoholic fatty liver tissues, Biosens. Bioelectron. 240 (2023) 115646.
[30] J.E. Rosenberger, Y.X. Xie, Y.Z. Fang, X. Lyu, W.S. Trout, O. Dmitrenko, et al., Ligand-directed photocatalysts and far-red light enable catalytic bioorthogonal uncaging inside live cells, J. Am. Chem. Soc. 145 (2023) 6067–6078.
[31] B.R. Cheng, L. Cao, C. Li, F.Y. Huo, Q.F. Meng, G.L. Tong, et al., Fluorine-doped carbon quantum dots with deep-red emission for hypochlorite determination and cancer cell imaging, Chin. Chem. Lett. 35 (2024) 108969.
[32] D.M. Fernandez, A.H. Rahman, N.F. Fernandez, A. Chudnovskiy, E.D. Amir, L. Amadori, et al., Single-cell immune landscape of human atherosclerotic plaques, Nat. Med. 25 (2019) 1576–1588.

Jingkang Li is currently a Ph.D. student in College of Chemistry, Jilin University. His interest is spectral analysis.

Mo Ma is currently a Ph.D. student in School of Pharmacy, Jilin University. His interest is spectral analysis.

Siqi Zhang is currently a Ph.D. student in College of Chemistry, Jilin University. His interest is spectral analysis.

Wenping Dong is currently a master degree student in College of Chemistry, Jilin University. Her interest is spectral analysis.

Pinyi Ma received his doctor's degree from College of Chemistry, Jilin University in 2017 and he is an associate professor in that school. His research area is spectral analysis.

Ziwei Zhang received her Ph.D. degree in biophysics in Cornell University in 2010. She is currently an associate professor in Jilin University. Her research interest focuses on spectral analysis and electron spin resonance spectroscopy.

Daqian Song received his doctor's degree from College of Chemistry, Jilin University in 2003 and he is a professor in that school. His research areas are spectral and chromatography analysis.